

Fault Modeling of Grid-forming Converters using Dynamic Phasor Theory

Zhang, Qi; Liu, Dong; Chen, Zhe

Published in:
2021 IEEE IAS Industrial and Commercial Power System Asia

DOI (link to publication from Publisher):
[10.1109/ICPSAsia52756.2021.9621633](https://doi.org/10.1109/ICPSAsia52756.2021.9621633)

Creative Commons License
CC BY 4.0

Publication date:
2021

Document Version
Accepted author manuscript, peer reviewed version

[Link to publication from Aalborg University](#)

Citation for published version (APA):
Zhang, Q., Liu, D., & Chen, Z. (2021). Fault Modeling of Grid-forming Converters using Dynamic Phasor Theory. In *2021 IEEE IAS Industrial and Commercial Power System Asia* (pp. 1011-1016). IEEE (Institute of Electrical and Electronics Engineers). <https://doi.org/10.1109/ICPSAsia52756.2021.9621633>

General rights

Copyright and moral rights for the publications made accessible in the public portal are retained by the authors and/or other copyright owners and it is a condition of accessing publications that users recognise and abide by the legal requirements associated with these rights.

- Users may download and print one copy of any publication from the public portal for the purpose of private study or research.
- You may not further distribute the material or use it for any profit-making activity or commercial gain
- You may freely distribute the URL identifying the publication in the public portal -

Take down policy

If you believe that this document breaches copyright please contact us at vbn@aub.aau.dk providing details, and we will remove access to the work immediately and investigate your claim.

Fault Modeling of Grid-forming Converters using Dynamic Phasor Theory

Qi Zhang

*Department of Energy Technology
Aalborg University
Aalborg, Denmark
qzg@et.aau.dk*

Dong Liu

*Department of Energy Technology
Aalborg University
Aalborg, Denmark
liucen1985@gmail.com*

Zhe Chen

*Department of Energy Technology
Aalborg University
Aalborg, Denmark
zch@et.aau.dk*

Abstract—It has been pointed out in recent years that grid-following and grid-supporting converters are harmful to the stability of the power system, and grid-forming converters (GFM) are becoming to be the most promising grid-connected converters for the integration of renewable energy. Nevertheless, the development of GFM converters challenges the fault analysis of the power system because GFM converters have a totally different fault response with that of the grid-supporting, grid-following converter, and the synchronous generator. The fault modeling of GFM converters is a foundation to overcome this issue, so it should be investigated firstly. However, this topic is rarely discussed in the previous literature. In order to fill this research gap, this paper proposes a fault modelling method for GFM converters based on the dynamic phasor theory. The dynamic phasor model of GFM converters can provide an effective interface to the power system analysis. Thus, the proposed model is outstanding because of its ability to analyze the interaction between converters and the power system in the fault analysis. To verify the correctness of the proposed model, a 12 MVA grid-forming converter is established in MATLAB/Simulink. The simulation results show that the proposed model can almost perfectly handle the fault analysis of the grid-forming converter.

Index Terms—Fault modeling, grid-forming converter, renewable energy, dynamic phasor theory.

I. INTRODUCTION

Grid-connected converters as the interface equipment of renewable energy generations push the modern power system into power electronics dominated systems (PEDS) [1]. In comparison with traditional synchronous generators, the disparate fault response of grid-connected converters results in new fault conditions to the operation and protection of PEDS [2]. Thus, it brings a new challenge to the fault analysis theory and the protection system design because the traditional fault analysis for synchronous generators is not applicable for that of grid-connected converters. Therefore, the traditional fault analysis theory should be further expanded to handle the challenge caused by new fault conditions caused by grid-connected converters.

Generally, based on the control strategies, grid-connected converters can be divided into three classes: grid-forming (GFM), grid-supporting (GST), and grid-following (GFL) converters. For GST and GFL converters, they work under a

stable voltage provided by the power grid and are normally controlled as a PQ node in the power system, so the interaction between these converters and the grid is weak. In contrast, GFM converters are designed to support the voltage of the grid, which means that the interaction between converters and the grid are strong. Consequently, GFL and GST converters are widely used in the power system at the beginning of development of renewable energy integration. However, in recent years, some studies has pointed out that, the GST and GFL converter are harmful to the stability of the power system, especially for the weak grid [1], [2], [6]. Under this content, the GFM converter is becoming the most promising candidate for the renewable energy integration of power system. For the widespread deployment of the GFM converter, it is very critical to grasp the fault behavior, fault response, and the fault characteristics.

As the foundation of the fault analysis theory, fault modeling of grid elements aims to provide simple and correct models to analyze the fault response of grid elements. Compared with traditional synchronous generators, fault responses of grid-connected converters are more complicated because of the fast-response control and the deficiency in over-current capability [1], [3], which makes the development of the fault analysis model of GFL and GST more sophisticated. Because of the widespread usage in power system, the fault analysis model of GFL and GST converters have been discussed and proposed in previous studies. However, the fault modeling of GFM converters is rarely discussed, and the fault analysis model of GFM converters is becoming a critical topic with the increasing amount of GFM converters connected to the grid.

In order to fill the research gap, this paper proposes the fault analysis model of GFM by using the dynamic phasors. Firstly, the V/F droop control strategy of GFM converters is overviewed. Secondly, the state-space dynamic phasor model of GFM converters is derived, in which the time-domain state-space model is established firstly and then the time-domain model is transformed into the dynamic phasor model.

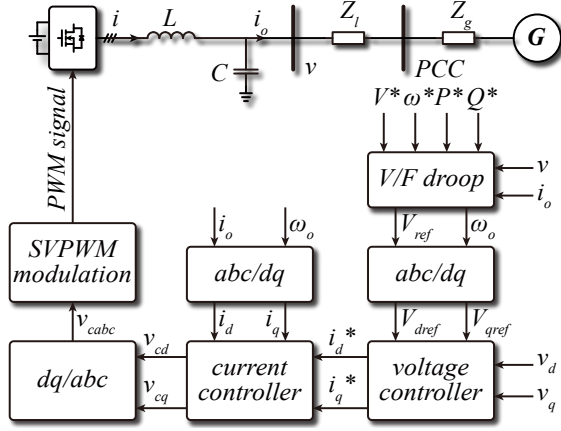


Fig. 1: The typical topology and the V/F control structure of the grid-forming converter.

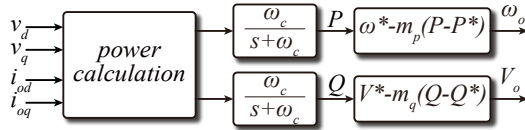


Fig. 2: The block diagram of the V/F droop controller.

II. FAULT MODELING OF GRID-FORMING CONVERTERS

A. Overview of the GFM and its control structure

The typical topology and general V/F droop control structure of GFM are shown in Fig. 1. The DC source and transformer of the grid-forming converter are assumed as ideal ones because the impact of them on the fault analysis can be ignored. Typically, the control system contains three parts: V/F droop based power controller, the voltage controller, and the current controller. The current controller controls the three-phase current flowing through the inductor labeled as i in Fig. 1, and the voltage controller is responsible for controlling the output voltage of GFM on the connection-port labeled as v . The output active and reactive power of GFM are controlled by the V/F droop controller and the reference input of the voltage controller is generated by the V/F droop controller. The block diagram of the V/F droop controller is shown in Fig. 2. Based on the structure of the V/F droop controller, the amplitude of the reference voltage V_o and the power angle ϕ of GFM can be expressed as (1).

$$\begin{cases} V_o = V^* - m_q(Q - Q^*) \\ \phi = \int 2\pi(\omega^* - m_p(P - P^*))dt \end{cases} \quad (1)$$

where: m_p, m_q are the droop coefficient of the droop controller.

B. Fault modeling of the GFM

The block diagram of the voltage and current controller is shown in Fig. 3. Take outputs of four PI controllers as state variables of the voltage and current controller, which are

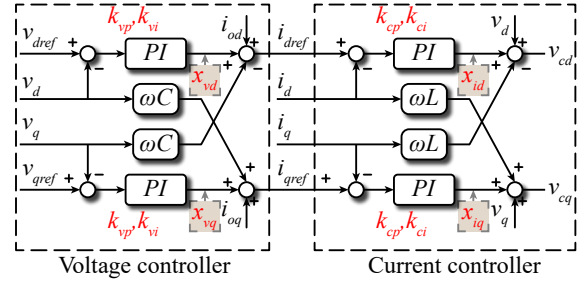


Fig. 3: The block diagram of the voltage and current controller. Note: the state-variables are labeled by red font with a rectangle background, and the parameters of PI controller are labeled by red font.

represented by $x_{vd}, x_{vq}, x_{id}, x_{iq}$, and labeled by red font with a rectangle background in Fig. 3. Subscripts v, i denote the states in the voltage and current controller, and subscripts d, q represent DQ components.

$$\begin{cases} \mathbf{x}_{vdq} = [x_{vd}, x_{vq}]^T \\ \mathbf{x}_{idq} = [x_{id}, x_{iq}]^T \end{cases} \quad (2)$$

Define the input and output of the voltage controller as:

$$\begin{cases} \mathbf{v}_{dqref} = [v_{dref}, v_{qref}]^T \\ \mathbf{v}_{dq} = [v_d, v_q]^T \\ \mathbf{i}_{dq} = [i_d, i_q]^T \\ \mathbf{i}_{odq} = [i_{od}, i_{oq}]^T \\ \mathbf{i}_{dqref} = [i_{dref}, i_{qref}]^T \end{cases} \quad (3)$$

Based on the structure of the voltage controller, the state-space model of the voltage controller can be obtained as (4). By the similar way, the model of the current controller can be obtained as (5).

$$\begin{cases} \dot{\mathbf{x}}_{vdq} = \mathbf{B}_1 \mathbf{v}_{dqref} + \mathbf{B}_2 \mathbf{v}_{dq} \\ \mathbf{i}_{dqref} = \mathbf{C}_1 \mathbf{x}_{vdq} + \mathbf{D}_1 \mathbf{v}_{dqref} + \mathbf{D}_2 \mathbf{v}_{dq} + \mathbf{D}_3 \mathbf{i}_{odq} \end{cases} \quad (4)$$

$$\begin{cases} \dot{\mathbf{x}}_{idq} = \mathbf{B}_1 \mathbf{i}_{dqref} + \mathbf{B}_2 \mathbf{i}_{dq} \\ \mathbf{v}_{cdq} = \mathbf{C}_2 \mathbf{x}_{idq} + \mathbf{D}_4 \mathbf{i}_{dqref} + \mathbf{D}_5 \mathbf{i}_{dq} + \mathbf{D}_3 \mathbf{v}_{dq} \end{cases} \quad (5)$$

where:

$$\begin{aligned} \mathbf{B}_1 &= \text{diag}(1, 1), \mathbf{B}_2 = -\text{diag}(1, 1) \\ \mathbf{C}_1 &= \text{diag}(k_{vi}, k_{vi}), \mathbf{C}_2 = \text{diag}(k_{ci}, k_{ci}) \\ \mathbf{D}_1 &= \text{diag}(k_{vp}, k_{vp}), \mathbf{D}_3 = \text{diag}(1, 1), \mathbf{D}_4 = \text{diag}(k_{cp}, k_{cp}) \\ \mathbf{D}_2 &= \begin{bmatrix} -K_{vp} & -\omega C \\ \omega C & -K_{vp} \end{bmatrix}, \mathbf{D}_5 = \begin{bmatrix} -K_{cp} & -\omega L \\ \omega L & -K_{cp} \end{bmatrix} \end{aligned} \quad (6)$$

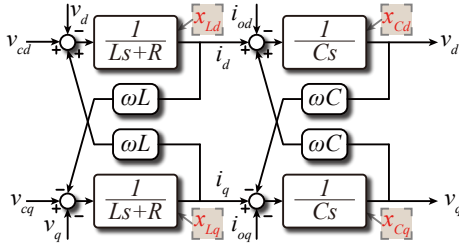


Fig. 4: The block diagram of the LC power filter.

Note: the state-variables are labeled by red fond with a rectangle background.

Combine (4) and (5), the time-domain state-space model of the controller can be obtained, which is shown in (7).

$$\begin{cases} p \begin{bmatrix} x_{vdq} \\ x_{idq} \end{bmatrix} = A_{ctr} \begin{bmatrix} x_{vdq} \\ x_{idq} \end{bmatrix} + B_{ctr} \begin{bmatrix} v_{dqref} \\ v_{dq} \\ i_{odq} \\ i_{dq} \end{bmatrix} \\ v_{cdq} = C_{ctr} \begin{bmatrix} x_{vdq} \\ x_{idq} \end{bmatrix} + D_{ctr} \begin{bmatrix} v_{dqref} \\ v_{dq} \\ i_{odq} \\ i_{dq} \end{bmatrix} \end{cases} \quad (7)$$

$$A_{ctr} = \begin{bmatrix} 0 & 0 \\ C_1 & 0 \end{bmatrix}, B_{ctr} = \begin{bmatrix} B_1 & B_2 & 0 & 0 \\ D_1 & D_2 & B_1 & B_2 \end{bmatrix} \\ C_{ctr} = [D_4 C_1], D_{ctr} = [D_1 D_4, D_3 + D_2 D_4, D_4, D_5]$$

where p is the differential operator. The block diagram of the model of the power filter is shown in Fig. 4. Define states variables of the inductor and the capacitor as $x_{Ld}, x_{Lq}, x_{Cd}, x_{Cq}$, which are labeled in Fig. 4, and define the output of the LC power filter as v_{dq}, i_{dq} :

$$\begin{cases} x_{Ldq} = [x_{Ld}, x_{Lq}]^T \\ x_{Cdq} = [x_{Cd}, x_{Cq}]^T \\ v_{dq} = [v_d, v_q]^T \\ i_{dq} = [i_d, i_q]^T \end{cases}$$

Based on the voltage-current relationship of inductors and capacitors, the time-domain model of the inductor and capacitor can be obtained as shown in (8) and (9).

$$\begin{cases} \dot{x}_{Ldq} = A_{L1} x_{Ldq} + B_{L1} v_{cdq} + B_{L2} v_{dq} \\ i_{dq} = C_{L1} x_{Ldq} \end{cases} \quad (8)$$

$$\begin{cases} \dot{x}_{Cdq} = A_{C1} x_{Cdq} + B_{C1} i_{dq} + B_{C2} i_{odq} \\ v_{dq} = C_{C1} x_{Cdq} \end{cases} \quad (9)$$

where:

$$A_{L1} = \begin{bmatrix} \frac{-R}{L} & \omega \\ -\omega & \frac{-R}{L} \end{bmatrix}, A_{C1} = \begin{bmatrix} 0 & \omega \\ -\omega & 0 \end{bmatrix} \\ B_{L1} = \text{diag}(1, 1), B_{L2} = -\text{diag}(1, 1) \\ B_{C1} = \text{diag}(1, 1), B_{C2} = -\text{diag}(1, 1) \\ C_{L1} = \begin{bmatrix} \frac{1}{L} & 0 \\ 0 & \frac{1}{L} \end{bmatrix}, C_{C1} = \begin{bmatrix} \frac{1}{C} & 0 \\ 0 & \frac{1}{C} \end{bmatrix}$$

Combine (8) and (9), the time-domain state-space model of the power filter can be obtained, which can be expressed as (10).

$$\begin{cases} p \begin{bmatrix} x_{Ldq} \\ x_{Cdq} \end{bmatrix} = A_{plt} \begin{bmatrix} x_{Ldq} \\ x_{Cdq} \end{bmatrix} + B_{plt} \begin{bmatrix} v_{cdq} \\ i_{odq} \end{bmatrix} \\ \begin{bmatrix} i_{dq} \\ v_{dq} \end{bmatrix} = C_{plt} \begin{bmatrix} x_{Ldq} \\ x_{Cdq} \end{bmatrix} \end{cases} \quad (10)$$

where:

$$A_{plt} = \begin{bmatrix} A_{L1} & C_{C1} \\ C_{L1} & A_{C1} \end{bmatrix}, B_{plt} = \begin{bmatrix} B_{L1} & 0 \\ 0 & B_{C2} \end{bmatrix} \\ C_{plt} = \begin{bmatrix} C_{L1} & 0 \\ 0 & C_{C1} \end{bmatrix}$$

According to the dynamic phasor theory [13], the dynamic phasor model of one three-phase voltage or current variable has a relationship with the DQ components, which can be expressed as (11).

$$x_{ph} = \frac{1}{2}(x_d + jx_q)e^{\frac{-j\pi}{2}} \quad (11)$$

where x_{ph} is the dynamic phasor model of a three-phase voltage or current, and x_d, x_q are their DQ components.

Combine (7) with (10), the time-domain state-space model of GFM can be obtained, and then the model can be transformed into the dynamic phasor model of GFM, based on the relationship defined as (11). The dynamic phasor model of GFM is expressed as (12).

$$\begin{cases} p \begin{bmatrix} \langle x_v \rangle_1 \\ \langle x_i \rangle_1 \\ \langle x_L \rangle_1 \\ \langle x_C \rangle_1 \end{bmatrix} = A_{ph} \begin{bmatrix} \langle x_v \rangle_1 \\ \langle x_i \rangle_1 \\ \langle x_L \rangle_1 \\ \langle x_C \rangle_1 \end{bmatrix} + B_{ph} \begin{bmatrix} \langle V_{ref} \rangle_1 \\ \langle i_o \rangle_1 \end{bmatrix} \\ \begin{bmatrix} \langle v \rangle_1 \\ \langle i \rangle_1 \end{bmatrix} = C_{ph} \begin{bmatrix} \langle x_v \rangle_1 \\ \langle x_i \rangle_1 \\ \langle x_L \rangle_1 \\ \langle x_C \rangle_1 \end{bmatrix} \end{cases} \quad (12)$$

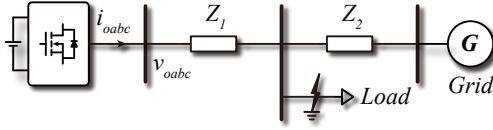


Fig. 5: The structure of the simulated test system.

TABLE I: Parameters of simulation model

Parameters	Values
Grid voltage	25 kV
Z_1 (positive sequence)	$0.1273 + j2.9333 \Omega$
Z_1 (negative sequence)	$3.864 + j12.964 \Omega$
Z_2 (positive sequence)	$0.6365 + j14.6665 \Omega$
Z_2 (negative sequence)	$19.32 + j64.820 \Omega$
Load	6 MW
Rated Power of GFM	12 MVA
Voltage of DC source	10 kV
System frequency	50 Hz
Resistance of the power filter	60 m Ω
Inductance of the power filter	4.2 mH
Capacitance of the filter	220 μ F
Cutoff frequency of current controller	1 kHz

where: $\langle x_v \rangle_1, \langle x_i \rangle_1, \langle x_L \rangle_1, \langle x_C \rangle_1, \langle V_{ref} \rangle_1, \langle i_o \rangle_1, \langle v \rangle_1, \langle i \rangle_1$ are transformed from $x_{vdq}, x_{idq}, x_{Ldq}, x_{Ldq}, v_{dqref}, i_{odq}, v_{dq}, i_{dq}$ respectively, based on (11). And:

$$A_{ph} = \begin{bmatrix} 0 & 0 & 0 & -\frac{1}{C} \\ k_{vi} & 0 & -\frac{1}{L} & -\frac{k_{vp}}{C} + j\omega \\ k_{cp}k_{vi} & k_{ci} & -\frac{k_{cp} + R}{L} & -\frac{k_{cp}k_{vp}}{C} + jk_{cp}\omega \\ 0 & 0 & \frac{1}{L} & -j\omega \end{bmatrix}$$

$$B_{ph} = \begin{bmatrix} 1 & 0 \\ k_{vp} & 1 \\ k_{cp}k_{vp} & k_{cp} \\ 0 & -1 \end{bmatrix}, C_{ph} = \begin{bmatrix} 0 & 0 & 0 & \frac{1}{C} \\ 0 & 0 & \frac{1}{L} & 0 \end{bmatrix}$$

The voltage frequency droop controller endows the GFM converter with a grid-supporting function. The amplitude and power angle generated by the V/F droop controller give the GFM converter the reference to control the output active and reactive power. Thus, compared with the slack bus, the power phase angle of the GFM converter is ϕ , and then the output voltage v_{oph} and current i_{oph} of the GFM converter can be expressed as (13).

$$\begin{cases} v_{oph} = \langle v \rangle_1 e^{j\phi} \\ i_{oph} = \langle i_o \rangle_1 e^{j\phi} \end{cases} \quad (13)$$

III. SIMULATION VERIFICATION

In order to verify the correctness of the proposed model, a 12 MVA GFM converter is established in MATLAB/Simulink. The structure of the test system in simulation is shown in Fig. 5. The converter is connected to an infinity power system

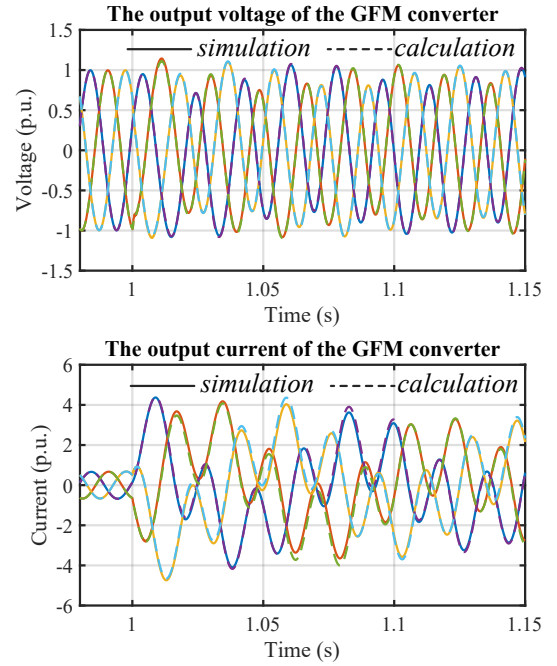


Fig. 6: The comparison result between the simulation and calculation when the three-phase to ground fault occurs.

through two transmission lines which are presented by Z_1, Z_2 . In the simulation, the π -network equivalent electric circuit model is used for the presentation of transmission lines. The topology and the control system of the GFM converter are shown in Fig. 1. The average model of the three-phase H-bridge in the GFM converter is used in the simulation, so the harmonics caused by the switching action are ignored. The detailed parameters of the simulation system are listed in Table. I. All measured voltages and currents in the simulation are per-unit based, and the base value of voltage and power are 25 kV and 12 MVA respectively.

The four normal kinds of fault including the three-phase to ground fault, the two-phase to ground fault, the two-phase short fault, and the single-phase to ground fault are analyzed by simulation and the proposed model, and the related result of the analysis are shown in Figs. 6 - 9. The output voltage and current of the GFM converter are recorded in the simulation, and they are also calculated by using the proposed model. For comparison, the simulation results are shown by the solid line, and the results calculated by the proposed model are highlighted by the dashed line in Figs. 6 - 9.

In all cases, the fault occurs at 1s. Before the fault occurrence, the converter works under normal conditions, in which the output voltage of the GFM converter is controlled to 1 p.u. and it injects rated power to the grid. After the faults, because of the voltage controller, the output voltage of the GFM converter only has a small disturbance but the output current increases seriously. Obviously, in all cases, the calculated results are almost perfectly consistent with the simulation results, which verifies the correctness of the

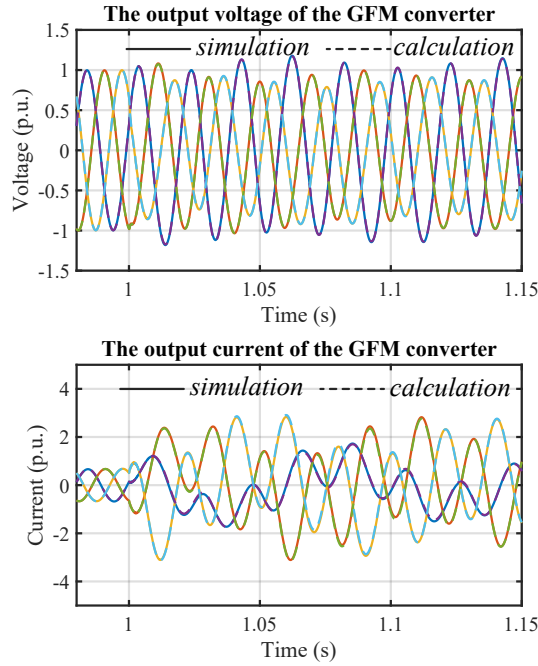


Fig. 7: The comparison result between the simulation and calculation when the two phase (phase B and C) to ground fault occurs.

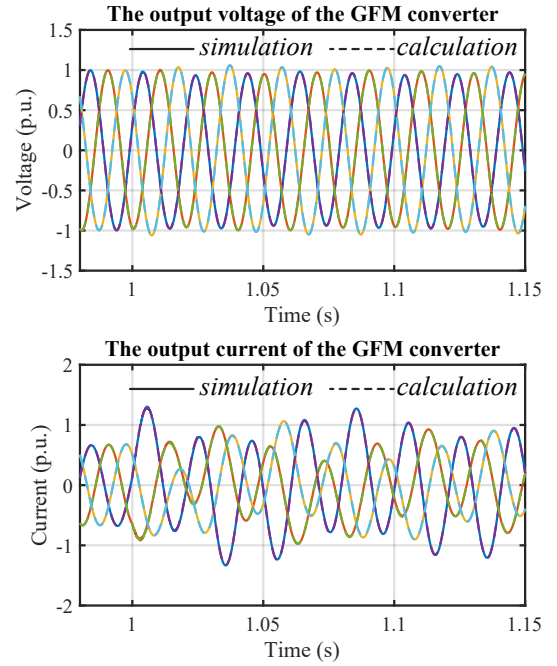


Fig. 9: The comparison result between the simulation and calculation when the single phase (phase A) to ground fault occurs.

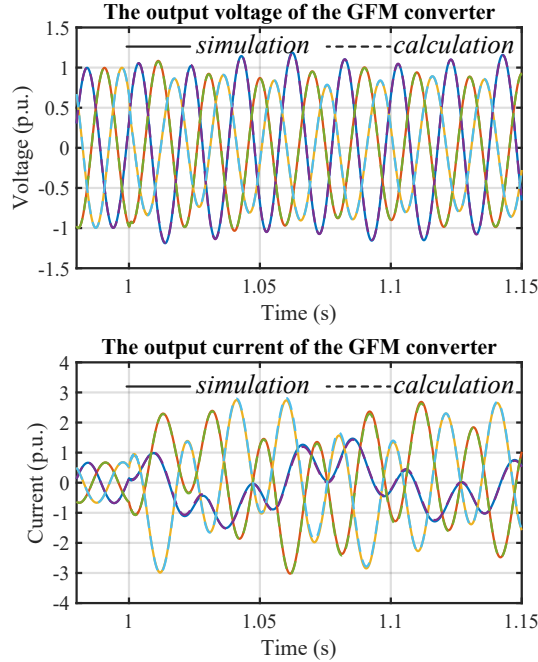


Fig. 8: The comparison result between the simulation and calculation when the two phase (phase B and C) short fault occurs.

proposed model.

IV. CONCLUSION

The fault response of GFM converters is different with that of the synchronous generator and other types of grid-connected converters. Thus, a new fault analysis model is required for the GFM converter. However, there is very limited research on it. In order to fill the research gap, this paper proposes a fault analysis model for the droop-controlled GFM converter based on the dynamic phasor theory. The proposed model has a major advantage that the interaction between the grid and converters can be analyzed simply due to the dynamic phasor theory. Especially for the fault analysis of the large-scale power system, such advantage of the proposed model is more obvious. The simulation result in MATLAB/Simulink verify the correctness of the proposed model.

In this paper, the low voltage ride through and the current limitation of the GFM converter are not considered in the proposed model, which will be further studied in our future work.

REFERENCES

- [1] "Impact of Inverter Based Generation on Bulk Power System Dynamics and Short-Circuit Performance," IEEE PES Industry Technical Support Task Force, PES-TR68, 2018. [online]. https://resourcecenter.ieee-pes.org/publications/technical-reports/PES_TR_7-18_0068.html.
- [2] G. Kou, L. Chen, P. VanSant, F. Velez-Cedeno and Y. Liu, "Fault Characteristics of Distributed Solar Generation," in IEEE Transactions on Power Delivery, vol. 35, no. 2, pp. 1062-1064, April 2020, doi: 10.1109/TPWRD.2019.2907462.
- [3] B. Kroposki et al., "Achieving a 100% Renewable Grid: Operating Electric Power Systems with Extremely High Levels of Variable Renewable Energy," in IEEE Power and Energy Magazine, vol. 15, no. 2, pp. 61-73, March-April 2017, doi: 10.1109/MPE.2016.2637122.

- [4] J. Rocabert, A. Luna, F. Blaabjerg and P. Rodriguez, "Control of Power Converters in AC Microgrids," in *IEEE Transactions on Power Electronics*, vol. 27, no. 11, pp. 4734-4749, Nov. 2012, doi: 10.1109/TPEL.2012.2199334.
- [5] D. Pattabiraman, R. H. Lasseter, and T. M. Jahns, "Comparison of Grid Following and Grid Forming Control for a High Inverter Penetration Power System," in *2018 IEEE Power and Energy Society General Meeting (PESGM)*, 5-10 Aug. 2018, pp. 1-5, doi: 10.1109/PESGM.2018.8586162.
- [6] I. Kim, "Short-Circuit Analysis Models for Unbalanced Inverter-Based Distributed Generation Sources and Loads," in *IEEE Transactions on Power Systems*, vol. 34, no. 5, pp. 3515-3526, Sept. 2019, doi: 10.1109/TPWRS.2019.2903552.
- [7] M. A. Azzouz and A. Hooshyar, "Dual Current Control of Inverter-Interfaced Renewable Energy Sources for Precise Phase Selection," in *IEEE Transactions on Smart Grid*, vol. 10, no. 5, pp. 5092-5102, Sept. 2019, doi: 10.1109/TSG.2018.2875422.
- [8] T. Kauffmann et al., "Short-Circuit Model for Type-IV Wind Turbine Generators With Decoupled Sequence Control," in *IEEE Transactions on Power Delivery*, vol. 34, no. 5, pp. 1998-2007, Oct. 2019, doi: 10.1109/TPWRD.2019.2908686.
- [9] W. Du et al., "Modeling of Grid-Forming and Grid-Following Inverters for Dynamic Simulation of Large-Scale Distribution Systems," in *IEEE Transactions on Power Delivery*, doi: 10.1109/TPWRD.2020.3018647.
- [10] M. E. Elkhatab, W. Du, and R. H. Lasseter, "Evaluation of Inverterbased Grid Frequency Support using Frequency-Watt and Grid-Forming PV Inverters," in *2018 IEEE Power and Energy Society General Meeting (PESGM)*, 5-10 Aug. 2018 2018, pp. 1-5, doi: 10.1109/PESGM.2018.8585958.
- [11] B. J. Pierre et al., "Bulk Power System Dynamics with Varying Levels of Synchronous Generators and Grid-Forming Power Inverters," in the *46th IEEE Photovoltaic Specialists Conference*, Chicago, Illinois, USA, 2019.
- [12] G. Denis, T. Prevost, M. S. Debry, F. Xavier, X. Guillaud, and A. Menze, "The Migrate project: the challenges of operating a transmission grid with only inverter-based generation. A grid-forming control improvement with transient current-limiting control," *IET Renewable Power Generation*, vol. 12, no. 5, pp. 523-529, 2018, doi: 10.1049/ietrpg.2017.0369.
- [13] S. R. Sanders, J. M. Noworolski, X. Z. Liu and G. C. Verghese, "Generalized averaging method for power conversion circuits," in *IEEE Transactions on Power Electronics*, vol. 6, no. 2, pp. 251-259, April 1991, doi: 10.1109/63.76811